

¹ Binocular combination in the autonomic nervous system

² Federico G. Segala^{1*}, Aurelio Bruno^{1,2}, Joel T. Martin^{1,3},
Anisa Y. Morsi¹, Alex R. Wade^{1,4} & Daniel H. Baker^{1,4}

³ ¹Department of Psychology, University of York, Heslington, York, YO10 5DD, United Kingdom.

⁴ ²School of Psychology and Vision Sciences, University of Leicester, Leicester, LE1 7RH, United Kingdom.

⁵ ³School of Philosophy, Psychology and Language Sciences, University of Edinburgh, Edinburgh, EH8 9AD,
⁶ United Kingdom.

⁷ ⁴York Biomedical Research Institute, University of York, Heslington, York, YO10 5NG, United Kingdom.

⁸ *Corresponding author

⁹ E-mail:federico.segala@york.ac.uk (FGS)

¹⁰ 1 Abstract

¹¹ Pupil diameters are regulated by the autonomic nervous system, which combines light signals across the eyes
¹² independently of the visual cortex. Distinct classes of retinal photoreceptor are involved in this process, with
¹³ cones and rods driving the initial constriction and intrinsically photosensitive retinal ganglion cells main-
¹⁴ taining diameter over prolonged time periods. We investigated binocular combination by targeting different
¹⁵ photoreceptor pathways using a novel binocular multiprimary system to modulate the input spectra via silent
¹⁶ substitution. At the first harmonic of the modulation frequency, luminance and S-cone responses showed
¹⁷ strong binocular facilitation, and weak interocular suppression. Melanopsin responses were invariant to the
¹⁸ number of eyes stimulated. Notably, the L-M pathway involved binocular inhibition, whereby responses to
¹⁹ binocular stimulation were weaker than for monocular stimulation. The second harmonic involved strong
²⁰ interocular suppression in all pathways, but with some evidence of binocular facilitation. Our results are
²¹ consistent with a computational model of binocular signal combination (implemented in a Bayesian hier-
²² archical framework), in which the weight of interocular suppression differs across pathways. We also find
²³ pathway differences in response phase, consistent with different lag times for phototransduction. This work
²⁴ demonstrates for the first time the algorithm governing binocular combination in the autonomic nervous
²⁵ system.

²⁶ 2 Author Summary

²⁷ Our pupils constantly adjust in size to control how much light enters the eye: in brighter conditions the pupils
²⁸ will reduce in size, and in dimmer conditions they will increase in size. This process, known as the pupillary
²⁹ light reflex, is usually taken for granted but is crucial for vision, and is controlled automatically by the body's
³⁰ nervous system. Different types of light-sensing cells in the retina contribute to this response: some respond
³¹ quickly to changes in light, while others maintain responses over longer periods. In our study, we explored
³² how signals from the two eyes are combined to regulate pupil size. Using a novel binocular light stimulator
³³ that allowed us to selectively target specific classes of photoreceptive cells separately in each eye, we found
³⁴ that the way the two eyes' signals are combined depends on which cell types are involved. For example,
³⁵ some cell classes showed cooperation between the eyes, while others showed competition. By revealing these
³⁶ distinct patterns of signal combination, our work provides new insight into how light information is integrated
³⁷ to regulate the pupils. A computational model built to summarize the results allows for comparisons within
³⁸ and between different sensory systems.

³⁹ **3 Introduction**

⁴⁰ The autonomic nervous system regulates many involuntary bodily processes, including the constriction and
⁴¹ dilation of the pupils in response to light [1]. The anatomical pathway from the retina to the subcortical
⁴² nuclei controlling the pupillary light response (PLR) is well established: it includes the Pretectal Olivary
⁴³ nucleus (PON), the Superior Cervical ganglion and the Edinger-Westphal nucleus, which project to the iris
⁴⁴ sphincter muscles that directly control the pupil size [1]. Evidence of a binocular component to the PLR is
⁴⁵ shown by the consensual response of the pupil (stimulation of one eye will cause constriction of the other
⁴⁶ eye) [2]. The anatomical segregation of the subcortical pathway from the rest of the brain means that this
⁴⁷ binocular combination of signals must occur independently of the cortical processes of binocular integration
⁴⁸ required for visual perception. Our recent work [3] has shown that the algorithm underlying binocular
⁴⁹ combination of light in the pupil pathway differs from that in the cortex. Here we extend this paradigm to
⁵⁰ compare binocular combination in different photoreceptor pathways that feed into the autonomic nervous
⁵¹ system.

⁵² Different classes of retinal photoreceptors, including cones, rods and melanopsin-containing intrinsically
⁵³ photosensitive retinal ganglion cells (ipRGCs), are directly involved in controlling and maintaining the size
⁵⁴ of the pupils [e.g. 4,5–8]. Cones drive the initial rapid constriction of the pupils [9], while the slower and
⁵⁵ longer activation of the ipRGCs maintains constriction over a prolonged period of time and regulates the
⁵⁶ post-illumination pupillary response [4,10]. The ipRGCs are a recently discovered photoreceptor class [11]
⁵⁷ that express the photopigment melanopsin, and are involved in the regulation of the circadian rhythm [12,13],
⁵⁸ forming a major input to the PON [14]. The first direct evidence of the involvement of the ipRGCs in the
⁵⁹ PLR was shown in melanopsin knockout rats [15], resulting in the loss of the intrinsic photosensitivity of
⁶⁰ the cells and a reduced pupil constriction. Similar behaviour was later observed in primates and humans
⁶¹ [16] using silent substitution (see Methods), where it was demonstrated that the PLR continues during light
⁶² presentation even when cone and rod signalling is blocked, indicating the primary role of the ipRGCs in
⁶³ maintaining pupil constriction over a prolonged time.

⁶⁴ Binocular combination has been extensively studied in visual perception, where it is mediated by neurons in
⁶⁵ primary visual cortex [17]. For pattern vision, binocular summation occurs at threshold, such that a lower
⁶⁶ contrast is required to detect a target shown to both eyes than a target shown to one eye [18,19]. At higher
⁶⁷ contrasts, the phenomenon of ‘ocularity invariance’ is observed, in which the response to monocularly- and
⁶⁸ binocularly-presented patterns is equal [20,21]. This is explained by a process of interocular suppression
⁶⁹ that cancels out the additional excitatory drive caused by stimulating two eyes. Our recent work [3] showed

70 that cortical signal combination for luminance flicker is substantially more linear than for spatial patterns,
71 whereas there is evidence of interocular suppression in the pupil pathway. Here we measure the amplitude
72 of pupil modulations in response to flickering stimuli presented as light flux, or directed towards the L-M
73 cone, S-cone, and melanopsin pathways (see Figure 1e-l). Our key comparisons are between monocular and
74 binocular stimulation, and in a dichoptic masking condition where the two eyes are stimulated at different
75 frequencies. The results are interpreted using a contemporary model of binocular vision [22] implemented
76 within a hierarchical Bayesian framework.

77 4 Results

78 Figure 1m-p shows averaged waveforms of pupil diameter in response to binocular stimulation. For light
79 flux stimuli (Figure 1m) a strong modulation is apparent at the stimulation frequency (0.5Hz), which is also
80 clear in the Fourier amplitude spectrum (Figure 1q). For binocular stimulation of the L-M pathway, S-cone
81 pathway and melanopsin pathway, pupil modulations were less than 10% of the amplitude of the light flux
82 modulation (note the change in y-axis scale for the Fourier spectra), but still apparent at 0.5Hz in the Fourier
83 spectra (Figure 1n-p). We also observed a second harmonic response (at 1Hz) for all conditions, which was
84 weaker than the first harmonic for light flux and melanopsin stimulation, but stronger for L-M and S-cone
85 stimulation. The second harmonic is also apparent in the pupil waveforms shown in Figure 1n-p. Our main
86 analysis therefore focuses on the amplitude of the pupil modulations at both the first and second harmonic
87 frequencies across different stimulus conditions.

88 Figure 2a-d shows contrast response functions across stimulation conditions for responses at the first harmonic
89 of the main stimulation frequency (0.5Hz). In each plot, the response to monocular stimulation is given by
90 the red circles and typically increases monotonically as a function of stimulus (temporal) contrast. Relative
91 to monocular stimulation, binocular stimulation led to higher response amplitudes, indicating a binocular
92 facilitation effect, for the light flux and S-cone conditions (Figure 2a,c), and to some extent for the melanopsin
93 condition (Figure 2d). However, the L-M cone condition (Figure 2b) produced a binocular suppression effect,
94 where the response to binocular stimulation was weaker than the response to monocular stimulation (blue
95 squares below red circles). These results indicate that the magnitude of binocular facilitation differs across
96 photoreceptor pathway, suggesting heterogeneity in the underlying neural computation.

97 In contemporary models of binocular signal combination, the amount of binocular facilitation is determined
98 by the magnitude of interocular suppression, with strong suppression reducing facilitation [23]. We can
99 estimate the strength of interocular suppression by measuring how much monocular responses are reduced

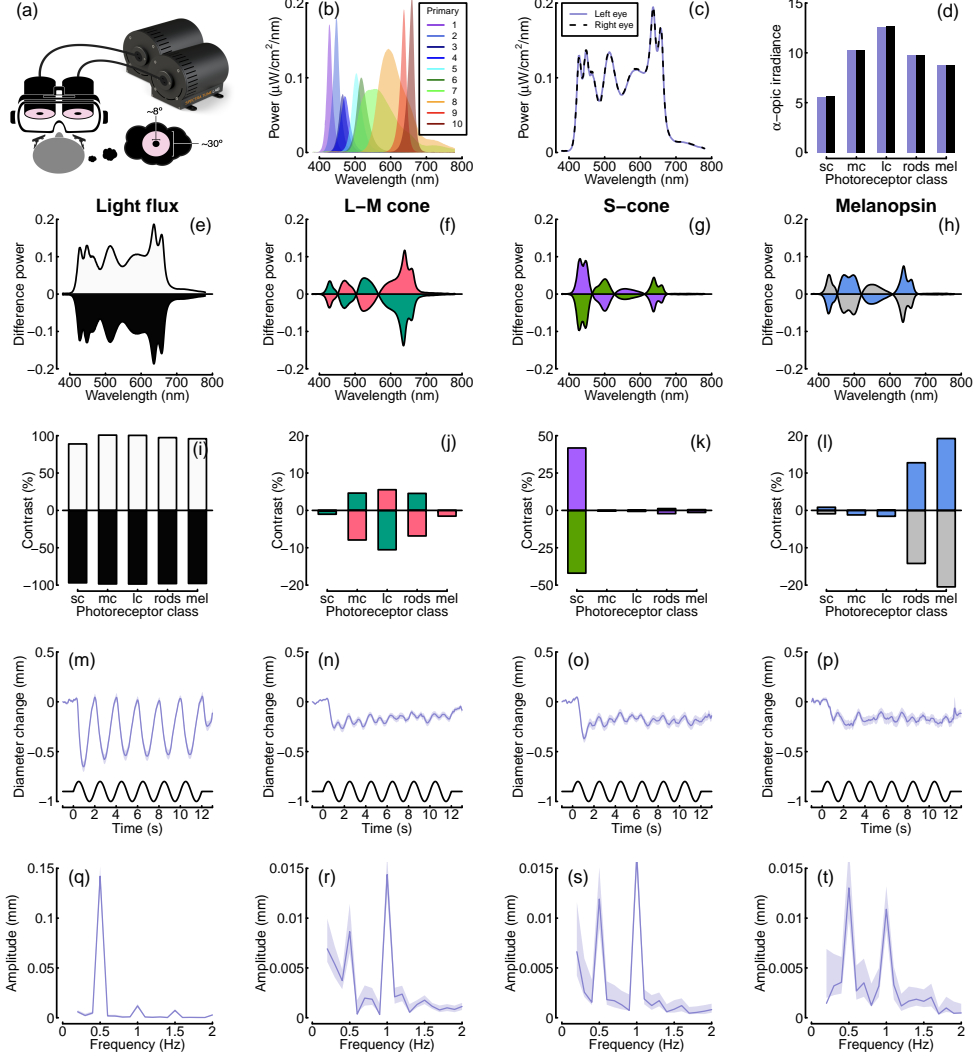


Figure 1: Summary of the spectral power distributions and alpha-optic irradiances for the background and each condition, as well as averaged pupil diameters and Fourier spectra. Panel (a) shows a schematic of the binocular stimulation system for presenting spectrally tuned modulations independently to each eye. The VR headset was attached to a clamp stand that the experimenters could use to adjust the height and align the headset with the eyes of the participant. The participant's head was supported by a chin rest to keep it in position throughout the experiment. Panel (b) shows the outputs of each LED primary at maximum intensity, and panels (c) and (d) show the overall spectral power distributions and the alpha-optic irradiances of the background spectra used for both eyes. The subsequent rows show the power differences (e-h), and photoreceptor contrasts (i-l) relative to the background, averaged pupil diameter waveforms (m-p) and Fourier spectra (q-t) for binocular stimulation. Column headings indicate the pathway stimulated, and shaded regions in panels m-t indicate bootstrapped 95% confidence intervals.

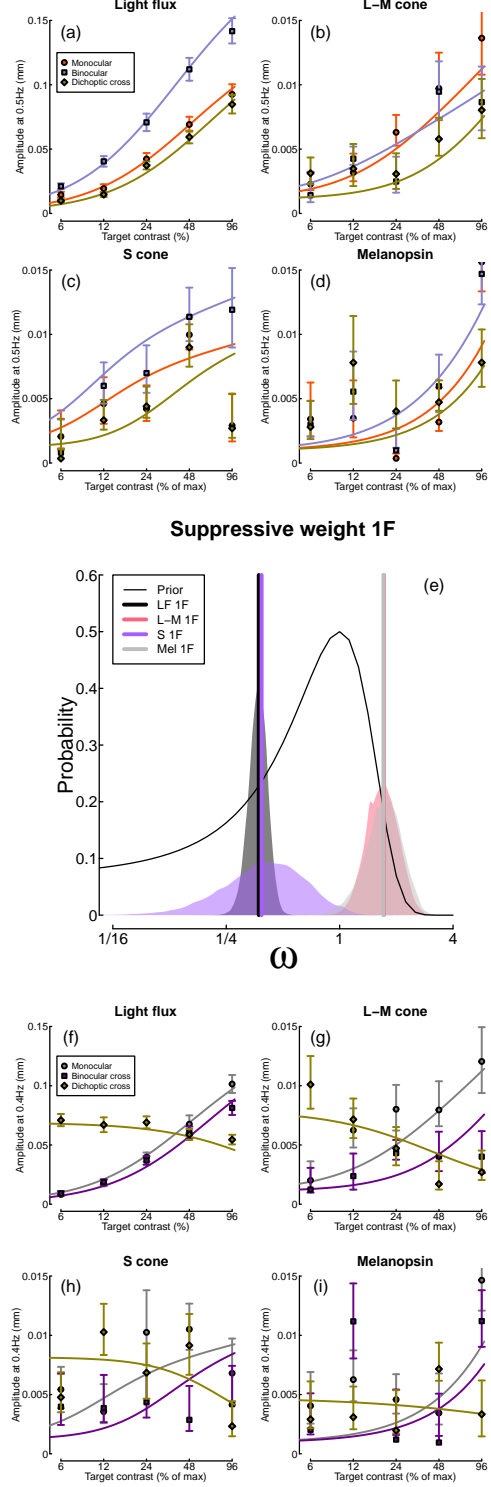


Figure 2: Contrast response functions for pupil modulations in response to flicker at 0.5Hz (panels a-d), and 0.4Hz (panels f-i), and posterior parameter distributions for the weight of interocular suppression (panel e). Within each panel (except panel e), data points are the coherently averaged amplitudes for each condition, and error bars indicate bootstrapped 95% confidence intervals. Curves show model fits using the maximum a posteriori (MAP) parameter values (see Table 1). In panel (e), vertical lines show the MAP estimates, and the thin black curve indicates the prior (note the logarithmic x-axis).

100 when a dichoptic ‘mask’ is shown to the other eye. In our paradigm, the two components flickered at different
 101 frequencies (0.5 and 0.4Hz) so that their responses remained distinct in the Fourier spectrum [e.g. 24]. The
 102 yellow diamond symbols in Figure 2a-d show the target responses in this condition, and in most cases were
 103 weaker than the monocular responses (red circles). The strongest dichoptic masking is found in the L-M
 104 condition, where we also observed the binocular suppression effect. Suppression can also be estimated from
 105 the responses at 0.4Hz (Figure 2f-i). The reduced amplitude in the binocular cross condition (where the
 106 two eyes received different temporal frequencies; purple squares) relative to the 0.4Hz monocular condition
 107 (grey circles), and the progressive decline in amplitude of the dichoptic cross response (yellow diamonds)
 108 also differ across photoreceptor conditions, showing similar differences to those observed at 0.5Hz.

109 To estimate the extent of interocular suppression for each photoreceptor pathway, we fitted each data set
 110 using a Bayesian hierarchical implementation of a simple binocular combination model [3,22]. Our primary
 111 objective was to compare posterior distributions of the weight of interocular suppression, which are shown in
 112 Figure 2e. Consistent with our earlier observations, the strongest suppressive weight corresponds to the L-M
 113 and Melanopsin conditions, and the weakest suppression corresponds to the light flux and S-cone conditions,
 114 with virtually no overlap between the posterior distributions for weak and strong suppression. The model
 115 fits were of good quality, as shown by the curves in Figure 2a-d,f-i. The fitted model parameters are given
 116 in Table 1.

Table 1: Summary of maximum a posteriori (MAP) parameter estimates for each data set.

Experiment	Z	k	w	p	q	Rmax
Light flux 1F	95.77	0.00083	0.37	1.32	1.24	0.0905
L-M cone 1F	49.82	0.00109	1.71	1.50	1.21	0.0032
S cone 1F	63.00	0.00121	0.39	1.94	1.79	0.0042
Melanopsin 1F	79.61	0.00094	1.71	1.29	0.76	0.0025
Light flux 2F	48.81	0.00089	1.24	1.15	0.88	0.0039
L-M cone 2F	66.00	0.00075	0.95	1.10	0.82	0.0050
S cone 2F	75.94	0.00097	2.22	1.41	0.83	0.0018
Melanopsin 2F	67.94	0.00101	1.37	0.90	0.49	0.0035

117 At the second harmonic frequencies, the levels of suppression were more uniform across different photore-
 118 ceptor pathways (see Figure 3). In general, suppression estimates were near or above 1 (see lower rows of
 119 Table 1), with substantial overlap between the posterior distributions (Figure 3e). The contrast response

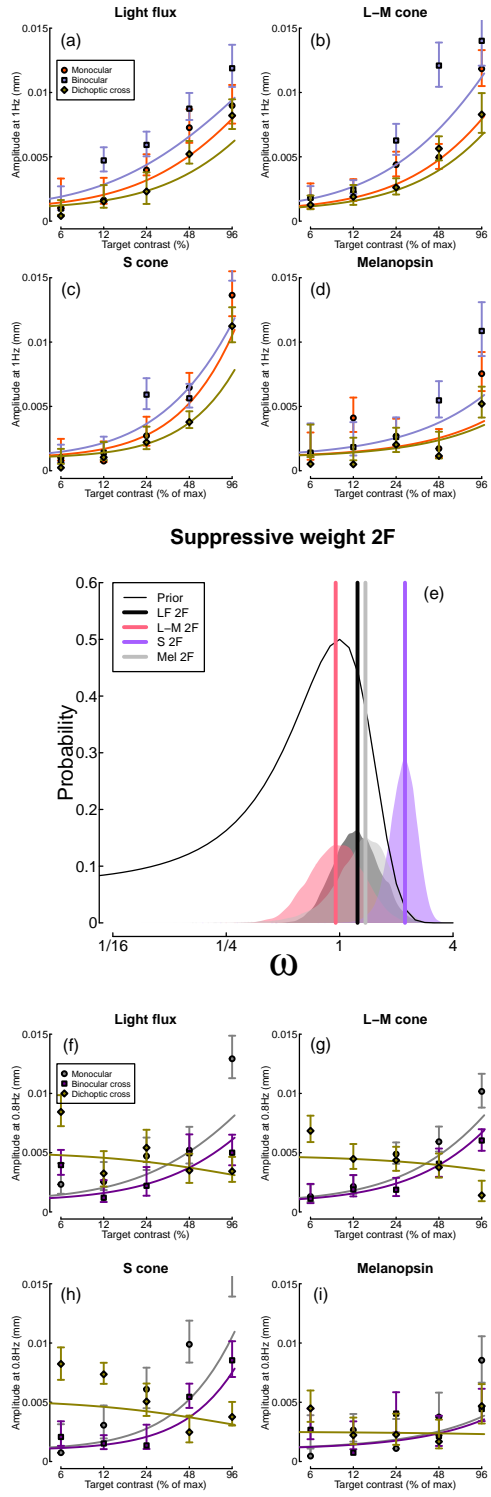


Figure 3: Responses at the second harmonic frequencies (1Hz and 0.8Hz), in the same format as Figure 2.

120 functions also looked more uniform, and generally involved less binocular facilitation and more interocular
 121 suppression than were seen at the first harmonics. The L-M condition now featured the weakest suppressive
 122 weight, and the strongest binocular facilitation, which was the opposite pattern seen at the first harmonic.

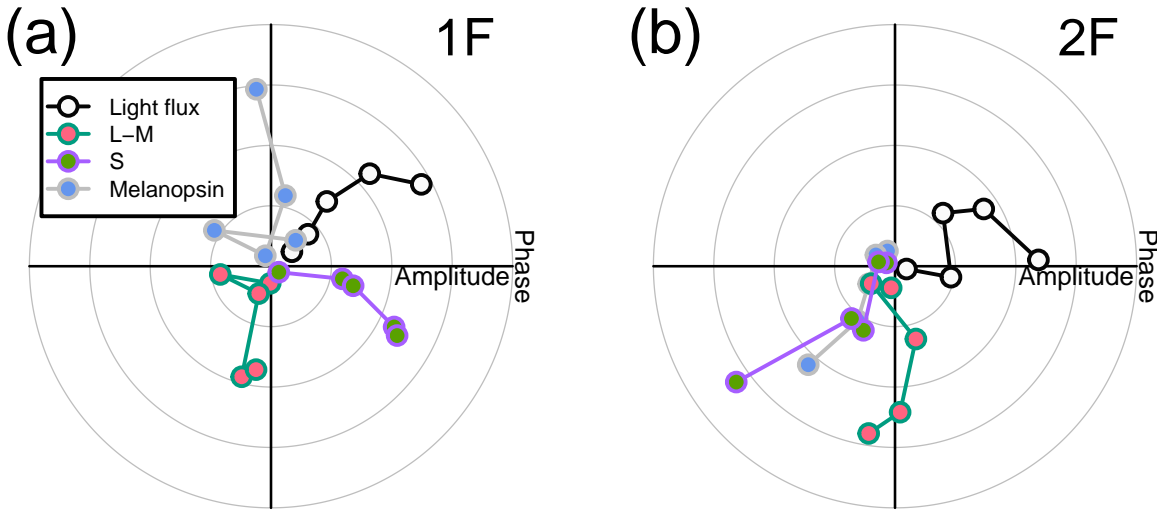


Figure 4: Pupil phase plots at the first and second harmonic frequencies for the light flux, melanopsin, L-M pathway and the S-cone pathway conditions. Panel (a) shows the pupil response at the first harmonic frequency during binocular stimulation. Panel (b) shows the pupil response at the second harmonic frequency during binocular stimulation. The five data points for each pathway correspond to the five contrast levels displayed. In panel (a) the light flux amplitudes have been scaled down by a factor of 10 to enable comparison with the other conditions.

123 Finally, we inspected the response phase of our four stimulation conditions, given previous reports that
 124 these differ across pathways [7], and may be in antiphase for melanopsin and S-cone signals. Figure 4 shows
 125 the phase angles for the first (a) and second (b) harmonic frequencies for binocular stimulation (monocular
 126 stimulation produced very similar results). At the first harmonic, melanopsin and S-cone signals differed in
 127 phase by more than 90 degrees, though they were not fully in antiphase. The light flux and L-M responses
 128 were approximately in antiphase to each other, however this is likely due to our choice to modulate L+M- in
 129 the first half-cycle of the sine wave (corresponding to a luminance increase in the light flux condition), and
 130 L-M+ in the second half-cycle (corresponding to a luminance decrease in the light flux condition). Had we
 131 reversed this phase arrangement, we would likely have seen a close phase correspondence between the L-M
 132 and light flux conditions (another way to think about this is that L-cone decreases and M-cone increases
 133 are processed like luminance increases). Phase differences between the light flux, S-cone and melanopsin
 134 conditions are likely attributable to different lags in phototransduction at the earliest stage (i.e. in the
 135 retina). At the second harmonic frequency (Figure 4b), the light flux condition was again out of phase with

136 the other three, and was approximately in quadrature phase with the L-M condition, and in antiphase with
137 both the S-cone and melanopsin conditions (which were in phase with each other). We note that the marked
138 phase differences between conditions make the possibility that our results are dominated by rod activity
139 relatively unlikely (e.g. in the L-M and melanopsin conditions, which have very different phase profiles).

140 5 Discussion

141 We used binocular pupillometry and silent substitution to measure monocular and binocular responses of
142 the pupils to flickering stimuli when stimulating specific photoreceptor pathways. In all four experiments, we
143 were able to record contrast response functions at both the first and the second harmonic frequencies. All
144 experiments showed that binocular combination in the autonomic nervous system happens in a non-linear
145 manner, with evidence of different magnitudes of interocular suppression depending on the photoreceptor
146 pathway. This pattern of results was confirmed by a computational model, which allowed us to compare the
147 weight of interocular suppression for each pathway. We found that at the first harmonic frequency the L-M
148 and melanopsin pathways involved strong suppression, whereas the light flux and S-cone pathways involved
149 weaker suppression. Suppression was strong in all four pathways at the second harmonic frequency. Finally,
150 the phase of the pupil response revealed different lag times for the different pathways at the first and second
151 harmonic frequencies.

152 This is the first study to investigate binocular interactions in the melanopsin pathway directly. A previous
153 meta-analysis [25] indicated that there may be a substantial binocular facilitation effect in the circadian
154 pathway, as indexed by melatonin suppression (melatonin is a hormone released by the pineal gland; its
155 production is suppressed by exposure to bright light, particularly when the melanopsin-containing ipRGCs
156 are stimulated). In brief, monocular stimulation of the ipRGCs requires up to ten times the signal strength
157 to produce an equivalent effect to binocular stimulation. This superadditive effect implies an absence of
158 interocular suppression, and perhaps the presence of either a highly compressive nonlinearity, or an AND-style
159 neural operation. Our findings here are very different - we do not see substantial binocular facilitation effects
160 in response to melanopsin modulation, and our data indicate that interocular suppression is very strong.
161 Moreover, by measuring the full contrast response function, we can rule out compressive nonlinearities,
162 because the functions accelerate at both the first and second harmonic frequencies. The explanation for this
163 difference could be due to different anatomical pathways. Binocular combination in the circadian system
164 likely takes place in the suprachiasmatic nucleus, whereas in the pupil constriction circuit the Edinger-
165 Westphal nucleus is the most likely site of binocular integration [9]. Presumably these anatomical differences,
166 and the practical constraints of the two systems, lead to differences in response.

167 Our recent psychophysical work [26] has looked at binocular interactions in the L-M and S-cone pathways, and
168 compared these to the light flux pathway. Using a contrast discrimination paradigm with spatial modulations
169 of light flux and colour, we found equally strong interocular suppression in all three pathways [26]. This
170 is rather different from our pupillometry results here, which demonstrate weaker suppression in the light
171 flux and S-cone pathways than in the L-M pathway (see Figure 2). However, the current experiments
172 involve temporal modulations, which are quite distinct from the spatial modulations used in our previous
173 work [26]. Our other recent work [3] has shown that temporal luminance modulations involve much weaker
174 interocular suppression in the cortical response than do spatial luminance modulations [27]. These different
175 normalization processes might reflect different priorities for spatial and temporal vision. Spatial vision aims
176 to fuse images to provide binocular single vision, and benefits from ‘ocularity invariance’ [20], in which
177 visual appearance is constant when viewed with one eye or two. Temporal vision is critical for motion
178 perception, which can involve alternative binocular computations, such as calculating velocity differences
179 between the eyes [28]. Of course the present measurements were of pupil size, which may be subject to
180 different anatomical and functional constraints from those in the cortex. Future research should aim to
181 extend our current findings to perception using psychophysical approaches.

182 6 Conclusions

183 We have demonstrated that binocular combination of temporal flickering light in the autonomic nervous
184 system depends on the photoreceptor pathway stimulated. We were able to elicit pupil responses by stimu-
185 lating the periphery of the retina and we were able to record contrast response functions for all photoreceptor
186 pathways. While all pathways showed non-linear combination, they varied in how the signals are combined,
187 particularly in the weight of interocular suppression. This was strong ($\omega \geq 1$) for L-M and melanopsin
188 signals at the first harmonic, and all pathways at the second harmonic. Suppression was weaker ($\omega < 1$) in
189 the light flux pathway (consistent with previous work), and also for S-cone directed modulations.

190 7 Materials and methods

191 7.1 Participants

192 Twenty-four participants were recruited for each of the four experiments for a total of ninety-six adult
193 participants (28 male, 68 female), whose ages ranged from 18 to 41. All participants had normal or corrected
194 to normal vision, no known abnormalities of binocular or colour vision, and gave written informed consent.
195 Our procedures were approved by the Ethics Committee of the Department of Psychology at the University

¹⁹⁶ of York (identification number 184).

¹⁹⁷ **7.2 Apparatus & stimuli**

¹⁹⁸ To present synchronised stimulus modulations independently to each eye, two light engines (Spec-
¹⁹⁹ traTuneLAB, which are thermally stable across time with active cooling according to the manufacturers:
²⁰⁰ LEDMOTIVE Technologies, LLC, Barcelona, Spain), each with 10 independently addressable LED colour
²⁰¹ channels, were integrated into a customised binocular viewing system. The light engines were operated via
²⁰² a Python interface to their REST API [29], which supports synchronous launch and playback of spectral
²⁰³ sequences prepared in advance and stored in JSON format. A special command was commissioned from
²⁰⁴ LEDMOTIVE to allow two different stimulus files to be launched simultaneously from the two devices. The
²⁰⁵ synchronisation of the spectra from the two devices was tested and showed that they were synchronised to
²⁰⁶ within approximately 3ms.

²⁰⁷ When preparing the spectral sequences, the age of participants was used to account for the yellowing of
²⁰⁸ the lenses. We used the silent substitution technique [30] to selectively stimulate specific photoreceptor
²⁰⁹ classes. Silent substitution exploits the fact that each photoreceptor class has a distinct spectral tuning that
²¹⁰ overlaps with the others. Using a multiprimary system, in which the primaries (i.e. LEDs) have different
²¹¹ spectra, it is possible to target one class of photoreceptors while maintaining the others at a constant
²¹² activity level, effectively silencing them [31,32, this paper also offers a clear explanation of how to implement
²¹³ silent substitution]. We calculated silent substitution solutions using the *PySilSub* toolbox [33], using linear
²¹⁴ algebra. The outputs of the two light engines (see Figure 1b,c) were calibrated using an Ocean Optics
²¹⁵ Jaz spectroradiometer, which was wavelength-calibrated to an Argon lamp and intensity calibrated using
²¹⁶ a NIST-traceable light source. Each primary was also linearised using a polynomial fit (see Figure S1 for
²¹⁷ details). We used the 10-degree cone fundamentals [34], and estimates of melanopsin absorbance spectra
²¹⁸ from CIE S 026 (discussed in a previous paper [33]) to calculate α -opic irradiance.

²¹⁹ The output from the light engines was directed through liquid light guides (LLG3-8H: Thorlabs Ltd, Cam-
²²⁰ bridgeshire, UK) and diffused onto semi-opaque and highly diffusive white glass discs with a diameter of 50
²²¹ mm for even illumination (34-473: Edmund Optics, York, UK). The light guide gaskets were butt-coupled
²²² to the light engine diffusers with threaded adapters (SM1A9, AD3LLG: Thorlabs Ltd, Cambridgeshire,
²²³ UK) and the exiting ends of the light guides were mated with 51 mm depth optical cylinders (SM2L20:
²²⁴ Thorlabs Ltd, Cambridgeshire, UK) via appropriately threaded adapters (AD3LLG, SM2A6: Thorlabs Ltd,
²²⁵ Cambridgeshire, UK). The stimulus diffuser discs were retained at the front end of the optical cylinders
²²⁶ approximately 51 mm from the light source, at which distance the output beam was sufficiently dispersed to

227 afford even illumination of the diffuser when viewed from the front. To guarantee safe illumination levels, a
228 circular neutral-density filter with the same diameter of the white glass discs (50 mm) and an optical density
229 of 0.6 log units was placed in the optical path between the light source and the diffusers. A small circular
230 piece of blackout material with a diameter of approximately 8 degrees (10 mm) was positioned centrally on
231 the front of each diffuser disc to aid as a fusion lock, as a fixation point, and to occlude the fovea.

232 The diffuser discs were positioned in the objective planes of the lenses of a modified VR headset (SHINECON
233 SC-G01, Dongguan Shinecon Industrial Co. Ltd., Guangdong, China), which was used by the participants to
234 view the stimuli. The stimuli were two discs of flickering light with a diameter of approximately 30 degrees,
235 which were fused together into a cyclopean percept resembling a donut-shaped ring of light, similar to that
236 used in other studies [e.g., 5,6,7,35,36]. The VR headset modifications allowed for small adjustments to
237 account for individual differences in interpupillary distance and focal length. The use of this set up allowed
238 us to modulate the stimuli in three different ocular configurations, similar to the ones we used in our previous
239 study [3]: monocular, binocular and dichoptic. In the monocular configuration, the unstimulated eye still
240 saw a non-flickering disc of mean light flux. A schematic of the stimulation system is shown in Figure
241 1a. Pupillometry data were collected using a binocular Pupil Core eye-tracker headset (Pupil Labs GmbH,
242 Berlin, Germany [37]) running at 120 Hz, and the signals were recorded with the Pupil Capture software.

243 Our previous study [3] used a temporal frequency of 2Hz for foveal luminance flicker, and recorded EEG
244 data simultaneously with pupillometry. Initial pilot experiments indicated that this frequency was too high
245 to elicit measurable responses when stimulating individual photoreceptor pathways. For all experiments, we
246 therefore used a primary flicker frequency of 0.5Hz, as previous literature showed that this was slow enough
247 to elicit a pupil response from all photoreceptor classes [7]. We also focussed on only recording pupillometry
248 data as this frequency would be too slow to elicit steady-state EEG responses [38].

249 For all experiments, sinusoidal temporal modulations were presented against the same background spectrum
250 (matched between the eyes), which was used to achieve silent substitution in the three photoreceptor mod-
251 ulation experiments. The background spectra were defined by setting all channels to half maximum output
252 for the brighter of the two devices (STLab 1, left eye) and then using the STLab 1/STLab 2 calibration
253 ratio to find the equivalent settings for the companion device (STLab 2, right eye). The background spec-
254 trum illuminance was approximately 74 lux, or 68.5 cd/m². The spectral power distributions and α -opic
255 irradiances of the background spectra for both eyes are shown in Figure 1c-d.

256 Silent substitution stimuli were prepared and calibrated for each participant with custom Python software [33]
257 and Python scripts. Estimates of photoreceptor spectral sensitivities for each participant were constructed

258 from the known photopigment absorbance spectra [34], taking account of the peak axial density of the
259 respective photopigments, as well as lens [34,39,40] and macular pigment density [40,41], in accordance with
260 the field size and age-dependant CIEPO06 observer model [42]. The melanopic and rhodopic action spectra
261 of the 32-year-old standard observer were taken from CIE S 026 [43] and then adjusted for age-related lens
262 transmittance with a spectral correction function, in line with the standard. Macular pigment correction
263 was not applied to the rhodopic and melanopic action spectra because rods are not present at the fovea and
264 ipRGCs sit above the retinal pigment layer [44].

265 In the light flux experiment, the stimulus intensity was increased and decreased relative to the background,
266 which we expected to modulate all photoreceptor classes (see Figure 1e,i). In the L-M cone modulation
267 experiment, we used silent substitution to increase the L-cone activity, and simultaneously decrease the
268 M-cone activity, during the first half-cycle of the sine wave. In the second half-cycle the polarity of the
269 modulation reversed (see Figure 1f,j). The maximum available L-M contrast was approximately 10%. In the
270 S-cone modulation experiment, we increased and decreased S-cone-directed signals, whilst keeping activity
271 in the other photoreceptors constant (see Figure 1g,k). Our system allowed a maximum contrast of 45%.
272 Finally, in the melanopsin experiment, we modulated the activity of the melanopsin-containing intrinsically
273 photoreceptive retinal ganglion cells, whilst keeping cone activity constant (see Figure 1h,l). The maximum
274 available melanopsin contrast was 22%. We assume that the activity of rods was constant at the high
275 background luminance intensity used here, and so did not attempt to silence rod activity in any condition, as
276 this would have greatly reduced the available dynamic range. Splatter on nominally silenced photoreceptors
277 was very small (see Figure 1j-l), well below the levels that would be expected to generate measurable pupil
278 modulations, although we can observe that the rods may not be saturated in the L-M and melanopsin-
279 directed stimuli (Figure 1j and 1l) and could intrude in these two experiments. We also estimated activation
280 of penumbral L and M cones [5,35,45], which was minimal (≤ 1.5 contrast; less than splatter on the open-field
281 cones) for melanopsin-directed stimuli. We note that the temporal frequency of our modulation (0.5Hz) is
282 well below the range where penumbral cone activation can elicit visible percepts, and that such percepts
283 fade after around 1 second [35], and do not typically affect pupil responses [7].

284 7.3 Procedure

285 Before the start of each experiment, participants adjusted the objective planes of the lenses with the help
286 of the experimenter until the stimulus was in focus and they perceived the two pieces of blackout material
287 as one fused disc. Pupil responses to binocular temporal contrast modulations were examined in a factorial
288 design that combined six ocular conditions and five temporal contrast levels: 6, 12, 24, 48 and 96% of the

available dynamic range. This design, similar to that used in our previous studies [3,27,46], was applied in four separate experiments, each with a different mode of photoreceptor stimulation. In the first three conditions, the discs flickered at 0.5 Hz, in either a monocular, binocular or dichoptic arrangement. In the dichoptic condition the non-target eye saw a flickering fixed contrast of 48% of the available dynamic range. In the remaining three conditions (the cross-frequency conditions) one eye's disc flickered at 0.4 Hz, and the other eye's disc flickered at 0.5 Hz. This included monocular responses at 0.4 Hz, as well as binocular (one eye sees each frequency at the target contrast) and dichoptic (target stimulus flickering at 0.5 Hz, mask contrast of 48% at 0.4 Hz in the other eye) arrangements. We counterbalanced presentation of the target stimulus across the left and right eyes.

The experiments were conducted in a windowless room, in which the only source of light was the modified VR headset. The participants sat as close as possible to the VR headset, leaving enough space for the eye-tracker to record the eyes. Each experiment was carried out in a single session of around 45-60 minutes, divided into three blocks of 15-17 minutes each. In each block, there were a total of 60 trials lasting 15 seconds each (12s of stimulus presentation, followed by 3s of interstimulus interval). The participants were given no task other than look at the black fixation dot while trying to minimise their blinking during the presentation period. For all experiments other than the light flux condition, participants adapted to the unmodulated background luminance for two minutes before stimulation began.

Before the start of the L-M experiment, participants completed a luminance nulling perceptual calibration procedure in L-M cone space on an Iiyama VisionMasterTM Pro 510 display (800 x 600 pixels, 60 Hz refresh rate). During the task, participants were presented with a disc flickering within the L-M cone space (between magenta and cyan). Using a trackball, participants adjusted the angle in cone space to find their subjective isoluminant point, which resulted in changing the flickering intensity of the stimulus until the amplitude of the flicker appeared to be minimised. The result was used to modify the requested contrasts during stimulus preparation so as to account for individual differences affecting perceived illuminance, principally the L:M cone ratio [47,48].

7.4 Data analysis

The pupillometry data were analysed using the same method we used in our previous study [3]. The data were converted from mp4 videos to a csv text file using the Pupil Player software [37], which estimated pupil diameter for each eye on each frame using a 3D model of the eyeball. The individual data were then loaded into R for analysis, where a ten-second waveform for each trial in each eye was extracted (excluding the first two seconds after stimulus onset). We interpolated across any dropped or missing frames to ensure

regular and continuous sampling over time. The Fourier transform was calculated for each waveform, and all repetitions of each condition were pooled across eye and then averaged. Finally, data were averaged across all participants to obtain the group results. We used coherent averaging and at each stage we excluded data points with a Mahalanobis distance exceeding $D = 3$ from the complex-valued mean [49]. For monocular stimulation, we confirmed that the consensual response was equivalent to the response in the stimulated eye.
 For all experiments, we used a bootstrapping procedure with 10^4 iterations to estimate standard errors across participants. All analysis and figure construction was conducted using a single R-script, available online, making this study fully computationally reproducible: <https://osf.io/gdvt4/>.

7.5 Computational model and parameter estimation

To quantitatively summarise our data, we used the same model described in our previous study [3]. The model has the same general form as the first stage of the contrast gain control model proposed by Meese and colleagues [22], but omits the second stage. For the previous model that we used [3], the exponent of the numerator and denominator had fixed values of 2 and (implicitly) 1. Here, we allow these parameters (called p and q) to be free, in order to permit different shapes of contrast response function, e.g. accelerating or saturating. The responses of the left eye and right eye channels are as follows:

$$resp_L = \frac{L^p}{Z + L^q + \omega R^q}, \quad (1)$$

$$resp_R = \frac{R^p}{Z + R^q + \omega L^q}, \quad (2)$$

where L and R are the contrast signals from the left and right eyes, p and q are exponents, Z is a saturation constant that shifts the contrast-response function laterally, and ω is the weight of suppression from the other eye.

The responses from the two eyes are then summed binocularly:

$$resp_B = R_{max}(resp_L + resp_R) + k, \quad (3)$$

where k is a noise parameter, and R_{max} scales the overall response amplitude.

The models were fit using a hierarchical Bayesian framework implemented in Stan [50]. The data for each

³⁴¹ photoreceptor type and response frequency was fit separately, for a total of 8 model fits. The prior for the ω
³⁴² parameter was Gaussian, with a mean of 1 and standard deviation of 0.5. Priors for the other free parameters
³⁴³ were also Gaussian, with mean values based on previous work [3]. We calculated over 10^6 posterior samples,
³⁴⁴ and retained 10% for plotting.

³⁴⁵ 8 References

- ³⁴⁶ 1. McDougal DH, Gamlin PD. Autonomic control of the eye. *Comprehensive Physiology*. 2015;5: 439–
³⁴⁷ 473. doi:[10.1002/cphy.c140014](https://doi.org/10.1002/cphy.c140014)
- ³⁴⁸ 2. Wyatt HJ, Musselman JF. Pupillary light reflex in humans: Evidence for an unbalanced pathway from
nasal retina, and for signal cancellation in brainstem. *Vision Res.* 1981;21: 513–25. doi:[10.1016/0042-6989\(81\)90097-3](https://doi.org/10.1016/0042-6989(81)90097-3)
- ³⁴⁹ 3. Segala FG, Bruno A, Martin JT, Aung MT, Wade AR, Baker DH. Different rules for binoc-
ular combination of luminance flicker in cortical and subcortical pathways. *eLife*. 2023;12.
³⁵¹ doi:[10.7554/elife.87048](https://doi.org/10.7554/elife.87048)
- ³⁵² 4. McDougal DH, Gamlin PD. The influence of intrinsically-photosensitive retinal ganglion cells on the
spectral sensitivity and response dynamics of the human pupillary light reflex. *Vision Research*.
³⁵³ 2010;50: 72–87. doi:[10.1016/j.visres.2009.10.012](https://doi.org/10.1016/j.visres.2009.10.012)
- ³⁵⁴ 5. Barrionuevo PA, Cao D. Luminance and chromatic signals interact differently with melanopsin acti-
³⁵⁵ vation to control the pupil light response. *Journal of Vision*. 2016;16(11): 29. doi:[10.1167/16.11.29](https://doi.org/10.1167/16.11.29)
- ³⁵⁶ 6. Murray IJ, Kremers J, McKeefry D, Parry NRA. Paradoxical pupil responses to isolated
M-cone increments. *Journal of the Optical Society of America A*. 2018;35: B66–B71.
³⁵⁷ doi:[10.1364/JOSAA.35.000B66](https://doi.org/10.1364/JOSAA.35.000B66)
- ³⁵⁸ 7. Spitschan M, Jain S, Brainard DH, Aguirre GK. Opponent melanopsin and s-cone signals in the human
pupillary light response. *Proceedings of the National Academy of Sciences*. 2014;111: 15568–15572.
³⁵⁹ doi:[10.1073/pnas.1400942111](https://doi.org/10.1073/pnas.1400942111)
- ³⁶⁰ 8. Woelders T, Leenheers T, Gordijn MCM, Hut RA, Beersma DGM, Wams EJ. Melanopsin- and L-
cone-induced pupil constriction is inhibited by S- and M-cones in humans. *Proceedings of the National
Academy of Sciences*. 2018;115: 792–797. doi:[10.1073/pnas.1716281115](https://doi.org/10.1073/pnas.1716281115)
- ³⁶² 9. Mathôt S. Pupilometry: Psychology, physiology, and function. *J Cogn.* 2018;1: 16.
³⁶³ doi:[10.5334/joc.18](https://doi.org/10.5334/joc.18)

- 364 10. Markwell EL, Feigl B, Zele AJ. Intrinsically photosensitive melanopsin retinal ganglion cell contributions to the pupillary light reflex and circadian rhythm. *Clinical and Experimental Optometry*.
365 2010;93: 137–149. doi:[10.1111/j.1444-0938.2010.00479.x](https://doi.org/10.1111/j.1444-0938.2010.00479.x)
- 366 11. Provencio I, Rodriguez IR, Jiang G, Hayes WP, Moreira EF, Rollag MD. A Novel Human Opsin
367 in the Inner Retina. *Journal of Neuroscience*. 2000;20: 600–605. doi:[10.1523/JNEUROSCI.20-02-00600.2000](https://doi.org/10.1523/JNEUROSCI.20-02-00600.2000)
- 368 12. Panda S, Sato TK, Castrucci AM, Rollag MD, DeGrip WJ, Hogenesch JB, et al. Melanopsin
369 (Opn4) requirement for normal light-induced circadian phase shifting. *Science*. 2002;298: 2213–2216.
doi:[10.1126/science.1076848](https://doi.org/10.1126/science.1076848)
- 370 13. Ruby NF, Brennan TJ, Xie X, Cao V, Franken P, Heller HC, et al. Role of melanopsin in circadian
371 responses to light. *Science*. 2002;298: 2211–2213. doi:[10.1126/science.1076701](https://doi.org/10.1126/science.1076701)
- 372 14. Dacey DM, Peterson BB, Robinson FR, Gamlin PD. Fireworks in the primate retina: In vitro
373 photodynamics reveals diverse LGN-projecting ganglion cell types. *Neuron*. 2003;37: 15–27.
doi:[https://doi.org/10.1016/S0896-6273\(02\)01143-1](https://doi.org/10.1016/S0896-6273(02)01143-1)
- 374 15. Lucas RJ, Hattar S, Takao M, Berson DM, Foster RG, Yau K-W. Diminished pupillary
375 light reflex at high irradiances in melanopsin-knockout mice. *Science*. 2003;299: 245–247.
doi:[10.1126/science.1077293](https://doi.org/10.1126/science.1077293)
- 376 16. Gamlin PDR, McDougal DH, Pokorny J, Smith VC, Yau K-W, Dacey DM. Human and macaque
377 pupil responses driven by melanopsin-containing retinal ganglion cells. *Vision Research*. 2007;47:
946–954. doi:[10.1016/j.visres.2006.12.015](https://doi.org/10.1016/j.visres.2006.12.015)
- 378 17. Hubel DH, Wiesel TN. Receptive fields, binocular interaction and functional architecture in the cat's
379 visual cortex. *J Physiol*. 1962;160: 106–54. doi:[10.1113/jphysiol.1962.sp006837](https://doi.org/10.1113/jphysiol.1962.sp006837)
- 380 18. Baker DH, Lygo FA, Meese TS, Georgeson MA. Binocular summation revisited: Beyond $\sqrt{2}$. *Psychol
381 Bull*. 2018;144: 1186–1199. doi:[10.1037/bul0000163](https://doi.org/10.1037/bul0000163)
- 382 19. Campbell FW, Green DG. Monocular versus binocular visual acuity. *Nature*. 1965;208: 191–2.
383 doi:[10.1038/208191a0](https://doi.org/10.1038/208191a0)
- 384 20. Baker DH, Meese TS, Georgeson MA. Binocular interaction: Contrast matching and con-
385 trast discrimination are predicted by the same model. *Spat Vis*. 2007;20: 397–413.
doi:[10.1163/156856807781503622](https://doi.org/10.1163/156856807781503622)
- 386 21. Moradi F, Heeger DJ. Inter-ocular contrast normalization in human visual cortex. *J Vis*. 2009;9:
387 13.1–22. doi:[10.1167/9.3.13](https://doi.org/10.1167/9.3.13)

- 388 22. Meese TS, Georgeson MA, Baker DH. Binocular contrast vision at and above threshold. *Journal of*
389 *Vision*. 2006;6: 1224–43. doi:[10.1167/6.11.7](https://doi.org/10.1167/6.11.7)
- 390 23. Kingdom FAA, Libenson L. Dichoptic color saturation mixture: Binocular luminance contrast pro-
391 motes perceptual averaging. *J Vis*. 2015;15: 2. doi:[10.1167/15.5.2](https://doi.org/10.1167/15.5.2)
- 392 24. Busse L, Wade AR, Carandini M. Representation of concurrent stimuli by population activity in
393 visual cortex. *Neuron*. 2009;64: 931–42. doi:[10.1016/j.neuron.2009.11.004](https://doi.org/10.1016/j.neuron.2009.11.004)
- 394 25. Spitschan M, Cajochen C. Binocular facilitation in light-mediated melatonin suppression? *J Pineal*
395 *Res*. 2019;67: e12602. doi:[10.1111/jpi.12602](https://doi.org/10.1111/jpi.12602)
- 396 26. Baker DH, Hansford KJ, Segala FG, Morsi AY, Huxley RJ, Martin JT, et al. Binocular integration
397 of chromatic and luminance signals. *J Vis*. 2024;24(12): 7. doi:[10.1167/jov.24.12.7](https://doi.org/10.1167/jov.24.12.7)
- 398 27. Baker DH, Wade AR. Evidence for an optimal algorithm underlying signal combination in human
399 visual cortex. *Cereb Cortex*. 2017;27: 254–264. doi:[10.1093/cercor/bhw395](https://doi.org/10.1093/cercor/bhw395)
- 400 28. Kaestner M, Maloney RT, Wailes-Newson KH, Bloj M, Harris JM, Morland AB, et al. Asymmetries
401 between achromatic and chromatic extraction of 3D motion signals. *Proc Natl Acad Sci U S A*.
2019;116: 13631–13640. doi:[10.1073/pnas.1817202116](https://doi.org/10.1073/pnas.1817202116)
- 402 29. Martin JT, Pinto J, Bulte D, Spitschan M. PyPlr: A versatile, integrated system of hardware and
403 software for researching the human pupillary light reflex. *Behavior Research Methods*. 2022;54:
2720–2739. doi:[10.3758/s13428-021-01759-3](https://doi.org/10.3758/s13428-021-01759-3)
- 404 30. Estévez O, Spekreijse H. The "silent substitution" method in visual research. *Vision Research*.
405 1982;22: 681–691. doi:[10.1016/0042-6989\(82\)90104-3](https://doi.org/10.1016/0042-6989(82)90104-3)
- 406 31. Shapiro AG, Pokorny J, Smith VC. Cone–rod receptor spaces with illustrations that use CRT phos-
407 phor and light-emitting-diode spectra. *Journal of the Optical Society of America A*. 1996;13: 2319.
doi:[10.1364/josaa.13.002319](https://doi.org/10.1364/josaa.13.002319)
- 408 32. Spitschan M, Woelders T. The Method of Silent Substitution for Examining Melanopsin Contributions
409 to Pupil Control. *Frontiers in Neurology*. 2018;9. doi:[10.3389/fneur.2018.00941](https://doi.org/10.3389/fneur.2018.00941)
- 410 33. Martin JT, Boynton GM, Baker DH, Wade AR, Spitschan M. PySilSub: An open-source python
411 toolbox for implementing the method of silent substitution in vision and nonvisual photoreception
research. *Journal of Vision*. 2023;23: 10. doi:[10.1167/jov.23.7.10](https://doi.org/10.1167/jov.23.7.10)
- 412 34. Stockman A, Sharpe LT. The spectral sensitivities of the middle- and long-wavelength-sensitive
cones derived from measurements in observers of known genotype. *Vision Res*. 2000;40: 1711–37.
doi:[10.1016/s0042-6989\(00\)00021-3](https://doi.org/10.1016/s0042-6989(00)00021-3)

- 413
- 414 35. Spitschan M, Aguirre GK, Brainard DH. Selective stimulation of penumbral cones reveals perception in
415 the shadow of retinal blood vessels. *PLoS One.* 2015;10: e0124328. doi:[10.1371/journal.pone.0124328](https://doi.org/10.1371/journal.pone.0124328)
- 416 36. Zele AJ, Feigl B, Adhikari P, Maynard ML, Cao D. Melanopsin photoreception contributes to human
417 visual detection, temporal and colour processing. *Scientific Reports.* 2018;8. doi:[10.1038/s41598-018-22197-w](https://doi.org/10.1038/s41598-018-22197-w)
- 418 37. Kassner M, Patera W, Bulling A. Pupil: An open source platform for pervasive eye tracking and mobile
419 gaze-based interaction. *Proceedings of the 2014 ACM international joint conference on pervasive and
ubiquitous computing: Adjunct publication.* ACM; 2014. doi:[10.1145/2638728.2641695](https://doi.org/10.1145/2638728.2641695)
- 420 38. Norcia AM, Appelbaum LG, Ales JM, Cottreau BR, Rossion B. The steady-state visual evoked
421 potential in vision research: A review. *Journal of Vision.* 2015;15(6): 4. doi:[10.1167/15.6.4](https://doi.org/10.1167/15.6.4)
- 422 39. Pokorny J, Smith VC, Lutze M. Aging of the human lens. *Applied Optics.* 1987;26: 1437.
423 doi:[10.1364/ao.26.001437](https://doi.org/10.1364/ao.26.001437)
- 424 40. Stockman A, Sharpe LT, Fach C. The spectral sensitivity of the human short-wavelength sensitive
425 cones derived from thresholds and color matches. *Vision Research.* 1999;39: 2901–2927. doi:[https://doi.org/10.1016/S0042-6989\(98\)00225-9](https://doi.org/10.1016/S0042-6989(98)00225-9)
- 426 41. Bone RA, Landrum JT, Fernandez L, Tarsis SL. Analysis of the macular pigment by HPLC: Retinal
427 distribution and age study. *Investigative Ophthalmology & Visual Science.* 1988;29: 843–849.
- 428 42. CIE. Fundamental chromaticity diagram with physiological axes. CIE Central Bureau; 2006. Available:
429 <https://cie.co.at/publications/fundamental-chromaticity-diagram-physiological-axes-part-1>
- 430 43. CIE. CIE system for metrology of optical radiation for ipRGC-influenced responses to light. CIE
431 Central Bureau; 2018. doi:[10.25039/S026.2018](https://doi.org/10.25039/S026.2018)
- 432 44. Trieschmann M, Kuijk FJGM van, Alexander R, Hermans P, Luthert P, Bird AC, et al. Macular
433 pigment in the human retina: Histological evaluation of localization and distribution. *Eye.* 2007;22:
132–137. doi:[10.1038/sj.eye.6702780](https://doi.org/10.1038/sj.eye.6702780)
- 434 45. Zele AJ, Adhikari P, Cao D, Feigl B. Melanopsin driven enhancement of cone-mediated visual pro-
435 cessing. *Vision Res.* 2019;160: 72–81. doi:[10.1016/j.visres.2019.04.009](https://doi.org/10.1016/j.visres.2019.04.009)
- 436 46. Baker DH, Vilidaite G, McClarnon E, Valkova E, Bruno A, Millman RE. Binaural summation of am-
437 plitude modulation involves weak interaural suppression. *Sci Rep.* 2020;10: 3560. doi:[10.1038/s41598-020-60602-5](https://doi.org/10.1038/s41598-020-60602-5)

- 438 47. Carroll J, Neitz J, Neitz M. Estimates of L:M cone ratio from ERG flicker photometry and genetics.
439 Journal of Vision. 2002;2: 1. doi:[10.1167/2.8.1](https://doi.org/10.1167/2.8.1)
- 440 48. Hofer H, Carroll J, Neitz J, Neitz M, Williams DR. Organization of the human trichromatic cone
441 mosaic. The Journal of Neuroscience. 2005;25: 9669–9679. doi:[10.1523/jneurosci.2414-05.2005](https://doi.org/10.1523/jneurosci.2414-05.2005)
- 442 49. Baker DH. Statistical analysis of periodic data in neuroscience. *Neurons, Behavior, Data analysis,
443 and Theory.* 2021;5. doi:[10.51628/001c.27680](https://doi.org/10.51628/001c.27680)
- 444 50. Carpenter B, Gelman A, Hoffman MD, Lee D, Goodrich B, Betancourt M, et al. Stan: A probabilistic
445 programming language. *J Stat Softw.* 2017;76. doi:[10.18637/jss.v076.i01](https://doi.org/10.18637/jss.v076.i01)

9 Supplementary material

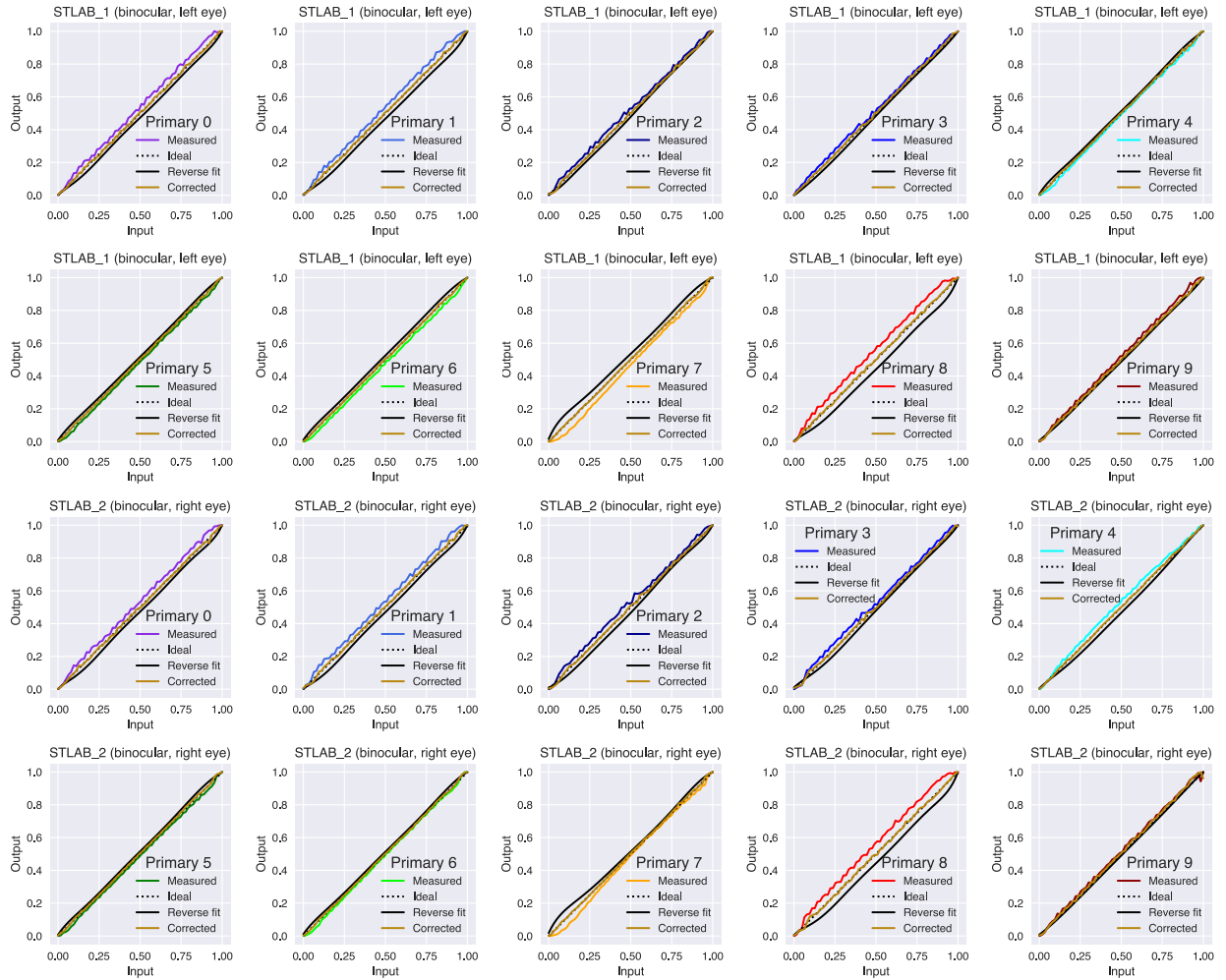


Figure S1: Linearity of primaries for each device. The calibration measures were summed (i.e., total unweighted irradiance), and the input-output relationship summarised by a 7th order polynomial reverse curve fit. By applying the coefficients of the regression, it is possible to achieve a linear output in the primaries.